



ELSEVIER

NeuroImage

www.elsevier.com/locate/ynimg  
NeuroImage xx (2005) xxx – xxx

1

## 2 A method to produce evolving functional connectivity maps during the 3 course of an fMRI experiment using wavelet-based time-varying 4 granger causality

5 João Ricardo Sato,<sup>a,\*</sup> Edson Amaro Junior,<sup>b</sup> Daniel Yasumasa Takahashi,<sup>b</sup>  
6 Marcelo de Maria Felix,<sup>b</sup> Michael John Brammer,<sup>c</sup> and Pedro Alberto Morettin<sup>a</sup>

7 <sup>a</sup>Institute of Mathematics and Statistics, University of São Paulo, Rua do Matão, 1010, Cidade Universitária, CEP 05508-090, São Paulo, S.P., Brazil

8 <sup>b</sup>Department of Radiology, University of São Paulo, Av. Dr. Enéas de Carvalho Aguiar, 255, 3o. andar, Cerqueira César, São Paulo, SP, CEP: 05403-001,  
9 São Paulo, S.P., Brazil

10 <sup>c</sup>Brain Image Analysis Unit, Institute of Psychiatry, King's College, London, De Crespigny Park, London SE5 8AF, UK

11 Received 10 August 2005; revised 22 November 2005; accepted 25 November 2005

12  
13

14 **Functional magnetic resonance imaging (fMRI) is widely used to**  
15 **identify neural correlates of cognitive tasks. Nevertheless, the analysis**  
16 **of functional connectivity is crucial to understanding neural dynam-**  
17 **ics. Although many studies of cerebral circuitry have revealed**  
18 **adaptative behavior, which can change during the course of the**  
19 **experiment, most of contemporary connectivity studies are based on**  
20 **correlations or structural equations analysis, assuming a time-**  
21 **invariant connectivity structure. In this paper, a novel method of**  
22 **continuous time-varying connectivity analysis is proposed, based on**  
23 **the wavelet expansion of functions and vector autoregressive model**  
24 **(wavelet dynamic vector autoregressive-DVAR). The model also**  
25 **allows identification of the direction of information flow between**  
26 **brain areas, extending the Granger causality concept to locally**  
27 **stationary processes. Simulation results show a good performance of**  
28 **this approach even using short time intervals. The application of this**  
29 **new approach is illustrated with fMRI data from a simple AB motor**  
30 **task experiment.**

31 © 2005 Elsevier Inc. All rights reserved.

32

33 *Keywords:* fMRI; Connectivity; Dynamic; Time-varying; Wavelets

34

### 35 Introduction

36 Functional neuroimaging using the BOLD (Blood Oxygen  
37 Level Dependent) effect has received considerable attention in the  
38 last decade and has become a powerful tool in cognitive  
39 neuroscience. Impressive methodological progress has been made  
40 since the first description of the effect (Ogawa et al., 1990) and a

41 large number of statistical methods for data analysis have been  
42 proposed, although most of them in somewhat ad hoc fashion. So  
43 far, image analysis reports in the literature are mainly dedicated to  
44 addressing the detection of brain activation. Such approaches  
45 (“brain mapping”), though very useful, are unable to address the  
46 more fundamental principles that characterize brain dynamics by  
47 probing the connectivity information obtainable from the BOLD  
48 signal.

49 Inferring the dynamics of interaction between different neural  
50 structures is a crucial step toward understanding neural organi-  
51 zation (Sameshima and Baccala, 1999; Friston, 2002). At  
52 conceptual level, there is active interest in the formulation of  
53 connectivity analysis. Friston has introduced the concept of  
54 dynamic causal models (DCM, Friston, 1995; Friston et al.,  
55 2003), based on nonlinear input-state-output systems, and a  
56 bilinear approximation to dynamic interactions. However, the  
57 DCM results rely on the prior connectivity specifications and also  
58 on stationarity conditions. A potentially promising approach to  
59 addressing some of these issues is the Granger causality concept  
60 (Granger, 1969; Sameshima and Baccala, 1999; Baccala and  
61 Sameshima, 2001; Roebroeck et al., 2005) which is borrowed  
62 from econometrics and based on the notion of the predictability  
63 of one signal by another, subject to the time constraint that the  
64 effect cannot precede the cause. It is specially suited to study  
65 partially ordered linear dependencies in multivariate contexts  
66 without assuming any prior connectivity structure. Recently,  
67 significant developments have occurred in the analysis of cerebral  
68 connectivity. Buchel and Friston (1997) introduced covariance  
69 structural equation modeling in fMRI applications. Subsequently,  
70 Goebel et al. (2003) and Roebroeck et al. (2005) have proposed  
71 the use of vector autoregressive models and shown their utility in  
72 the analysis of fMRI experiments. Nevertheless, Granger causal-  
73 ity alone is not sufficient to infer effective causal relations, as it is  
74 based only on predictive power. Recent developments in

\* Corresponding author. Rua Croata 774, ap22., Vila Ipojuca, São Paulo-  
S.P., CEP 05056-020, Brazil.

E-mail address: jsato@ime.usp.br (J.R. Sato).

Available online on ScienceDirect (www.sciencedirect.com).

graphical models have worked towards the identification of effective causal links. Eichler (2005) suggested a graphical representation of multivariate data that allows the inference of effective connectivity, even in the presence of latent variables.

In its original form, Granger causality was defined for linear stationary multichannel signals but, as with most biological signals, there is no unique model for fMRI data and no strong theoretical or experimental basis for the assumptions of stationarity of processes. It is widely recognized that incorrect use of these assumptions can lead to incorrect inferences.

Here, we propose a new method: the wavelet dynamic vector autoregressive (DVAR) process, which can be seen as a generalization of vector autoregressive model (VAR). This approach does not require assumptions about the direction of influence. The DVAR model is a multivariate version of the one proposed by Chang and Morettn (2005) and Dahlhaus et al. (1999). Its novel feature lies in directly modeling time-varying coefficients through wavelet bases with a balance between model complexity and interpretability. Wavelet analysis is an area of intense research in statistical signal analysis because of its wide applicability to model nonstationary signals and its deep relationship to time-frequency representation of a signal. Bullmore et al. (2003, 2004) have demonstrated the value of wavelet analysis applied to the BOLD signal as a means of retaining the colored-noise characteristics of the time series during permutation testing of statistical significance, thus highlighting the use of wavelet techniques in fMRI. Our aim was to combine wavelet analysis and the Granger causality concept given by VAR models to extend the methodology available for the study of brain connectivity. Fitting time-varying coefficients using a wavelet basis allowed us to model nonstationary (locally stationary) and nonlinear (locally linear) multichannel signals using Granger causal (VAR) approaches and make inferences about temporal dynamics of neural interactions. Thus, we can infer the connectivity structure of brain regions in a time-varying way.

In this article, a review of Granger causality theory and connectivity is presented, followed by the methodology underlying the new approach. Simulation results are presented and the usefulness of the method is illustrated in an application involving real fMRI data, in a simple sensorimotor experiment.

## 116 Granger causality and dynamic connectivity

Granger causality (Granger, 1969) is a concept that originated in the area of econometrics, focusing on understanding the relationships between two time series. Granger (1969) defined the causality in terms of predictability, based on the fact that the effect cannot come before the cause. Subsequently, Goebel et al. (2003) applied Granger causality to the description of interregional connectivity in fMRI data and to detection of the direction of information flow between brain regions.

Formally, consider a  $k$ -dimensional multivariate time series  $\mathbf{y}_t$

$$\mathbf{y}_t = [y_{1t} \ y_{2t} \ \dots \ y_{kt}]^T,$$

composed by  $k$  time series measured on time  $t$ . The Granger causality identification is based on the improvement in predictions of future values of the series  $\mathbf{y}_t$ , using the information of a collection of  $p$  past values of the series ( $\mathbf{y}_{t-1}, \mathbf{y}_{t-2}, \dots, \mathbf{y}_{t-p}$ ).

Hence, consider a  $k$ -dimensional vector autoregressive model (VAR) of order  $p$ , defined by

$$\mathbf{y}_t = \mathbf{v} + \mathbf{A}_1 \mathbf{y}_{t-1} + \mathbf{A}_2 \mathbf{y}_{t-2} + \dots + \mathbf{A}_p \mathbf{y}_{t-p} + \mathbf{u}_t,$$

where  $\mathbf{u}_t$  is an error vector of random variables with zero mean and covariance matrix  $\Sigma$  given by

$$\Sigma = \begin{bmatrix} \sigma_{11}^2 & \sigma_{21} & \dots & \sigma_{k1} \\ \sigma_{12} & \sigma_{22}^2 & \dots & \sigma_{k2} \\ \sigma_{13} & \sigma_{23} & \dots & \sigma_{k3} \\ \vdots & \vdots & \ddots & \vdots \\ \sigma_{1k} & \sigma_{2k} & \dots & \sigma_{kk}^2 \end{bmatrix},$$

and  $\mathbf{v}$  and  $\mathbf{A}_i$  ( $i = 1, 2, \dots, p$ ) are coefficient matrices given by

$$\mathbf{v} = \begin{bmatrix} v_1 \\ v_2 \\ \vdots \\ v_k \end{bmatrix} \quad \mathbf{A}_i = \begin{bmatrix} a_{11i} & a_{21i} & \dots & a_{k1i} \\ a_{12i} & a_{22i} & \dots & a_{k2i} \\ a_{13i} & a_{23i} & \dots & a_{k3i} \\ \vdots & \vdots & \ddots & \vdots \\ a_{1ki} & a_{2ki} & \dots & a_{kki} \end{bmatrix}.$$

The VAR model allows an easy way of identifying Granger causality. An important result of the VAR model, is that the series  $y_{jt}$  noncauses  $y_{it}$ , if and only if, the coefficient  $a_{ji} = 0$  for any  $i$ . In other words, the past values of  $y_{jt}$  aid the prediction of future values of  $y_{it}$ . Hence, Granger causalities can be identified simply looking for the VAR representation, and the direction of causality can be interpreted as the direction of information flow. Furthermore, Granger causality relationship is not necessarily reciprocal, for example,  $y_{jt}$  may Granger cause the signal  $y_{it}$ , without any implication that  $y_{it}$  Granger causes  $y_{jt}$ .

This approach can be extended to the analysis of time series of BOLD signals in functional magnetic resonance imaging data (Goebel et al., 2003). Let  $k$ -dimensional time series represent the regions of interest BOLD signal. Using the concept of Granger causality, the VAR modeling makes possible the identification of functional connectivity between brain areas by simply testing the significance of the estimates of the components of the matrix  $\mathbf{A}_i$ . However, as the Granger causality is defined in terms of predictability, the VAR modeling can indicate only functional relationships. In other words, this approach points out the links between signals, but does not, per se, indicate neurophysiologic mechanisms (effective connectivity).

There are two widely used approaches to assigning significance to the elements of matrices  $\mathbf{A}_i$ . The first is based on a Wald test for the statistical significance of the causality coefficients of a VAR model (Lütkepohl, 1993). The second one is based on the computation of F statistics by considering the ratio of residual variances and is described in detail by Geweke (1982).

According to Roebroeck et al. (2005), there are two main obstacles to the application of Granger causality mapping in fMRI. The first obstacle is that the BOLD response is not a direct measure of neural activity, and then, the connectivity relationships cannot be identified due to hemodynamic blurring. Furthermore, the low temporal resolution of fMRI may not provide enough information for inferring connectivity. Despite these apparent problems, the above authors were able to show by simulations that the Granger causality can be useful for inferring brain functional connectivity.

However, VAR modeling is an adequate approach only in cases of stationary time series, i.e., the autoregressive coefficients and error matrix covariance are time-invariant. In fact, most connectivity studies of fMRI data to date have used correlation analysis or structural equations models, assuming stationarity conditions. In

183 order to overcome this limitation, we propose a new approach  
184 using dynamic VAR (DVAR), defined by

$$\mathbf{y}_t = \mathbf{v}(t) + \mathbf{A}_1(t)\mathbf{y}_{t-1} + \mathbf{A}_2(t)\mathbf{y}_{t-2} + \dots + \mathbf{A}_p(t)\mathbf{y}_{t-p} + \mathbf{u}_t,$$

185 where  $\mathbf{u}_t$  is an error vector of random variables with zero mean and  
186 covariance matrix  $\Sigma(t)$  given by

$$\Sigma = \begin{bmatrix} \sigma_{11}^2(t) & \sigma_{21}(t) & \dots & \sigma_{k1}(t) \\ \sigma_{12}(t) & \sigma_{22}^2(t) & \dots & \sigma_{k2}(t) \\ \sigma_{13}(t) & \sigma_{23}(t) & \dots & \sigma_{k3}(t) \\ \vdots & \vdots & \ddots & \vdots \\ \sigma_{1k}(t) & \sigma_{2k}(t) & \dots & \sigma_{kk}^2(t) \end{bmatrix},$$

189 and  $\mathbf{v}(t)$  and  $\mathbf{A}_i(t)$  ( $i = 1, 2, \dots, p$ ) are coefficient matrices given by

$$\mathbf{v}(t) = \begin{bmatrix} v_1(t) \\ v_2(t) \\ \vdots \\ v_k(t) \end{bmatrix} \quad \mathbf{A}_i(t) = \begin{bmatrix} a_{11i}(t) & a_{21i}(t) & \dots & a_{k1i}(t) \\ a_{12i}(t) & a_{22i}(t) & \dots & a_{k2i}(t) \\ a_{13i}(t) & a_{23i}(t) & \dots & a_{k3i}(t) \\ \vdots & \vdots & \ddots & \vdots \\ a_{1ki}(t) & a_{2ki}(t) & \dots & a_{kki}(t) \end{bmatrix}.$$

190 In other words, in this case, we allow a time-variant structure  
193 for the intercept, autoregression coefficients and covariance matrix.  
194 Time-varying autoregressive models have previously been esti-  
195 mated using adaptative filters or windowed models. However,  
196 these approaches are suitable only in the context of time-series with  
197 many sample points. Many (probably most) fMRI data do not  
198 satisfy this criterion. Furthermore, the classical windowed models  
199 do not allow efficient estimation in cases of replications of  
200 conditions, as the AB periodic experiments. Here, a wavelet-based  
201 dynamic multivariate autoregression estimation is proposed, and its  
202 usefulness illustrated by simulations and an application to a real  
203 fMRI experiment.

## 204 A wavelet approach

205 Firstly, let an orthonormal basis generated by a mother wavelet  
206 function  $\psi(t)$ ,

$$\psi_{j,k}(t) = 2^{j/2}\psi(2^j t - k), \quad j, k \in \mathbb{Z},$$

208 and assume the following properties:

209

210 (i)  $\int_{-\infty}^{\infty} \psi(t) dt = 0$

211

212 (ii)  $\int_{-\infty}^{\infty} |\psi(t)| dt < \infty$

213

214 (iii)  $\int_{-\infty}^{\infty} \frac{|\Psi(\omega)|^2 d\omega}{|\omega|} < \infty$ , where the function  $\Psi(\omega)$  is the

215

216 Fouriertransform of  $\psi(t)$ .

217

218 (iv)  $\int_{-\infty}^{\infty} t^j \psi(t) dt = 0, j = 0, 1, \dots, r-1$  for  $r \geq 1$  and

219

220  $\int_{-\infty}^{\infty} t^j \psi(t) dt = 0.$

221

222

An important result is that any function  $f(t)$  with  $\int_{-\infty}^{\infty} f^2(t) dt < \infty$   
223 can be expanded as 225

$$f(t) = \sum_{j=-\infty}^{\infty} \sum_{k=-\infty}^{\infty} c_{j,k} \psi_{j,k}(t).$$

In other words, the function  $f(t)$  can be represented by a linear  
226 combination of functions  $\psi_{j,k}(t)$ . Therefore, considering the time-  
228 varying VAR model, the autoregressive coefficient functions  $a_{lmi}(t)$   
229 can be expanded as 230

$$a_{lmi}(t) = \sum_{j=-\infty}^{\infty} \sum_{k=-\infty}^{\infty} c_{j,k}^{(i)} \psi_{j,k}(t).$$

In practice, we use a truncated wavelet expansion, given by 231

$$a_{lmi}(t) = c_{-1,0}^{(i)} \phi(t) + \sum_{j=0}^J \sum_{k=0}^{2^j-1} c_{j,k}^{(i)} \psi_{j,k}(t).$$

where the time series extension  $T$  is a power of two,  $\phi(t)$  is  
234 called the scale function and  $c_{j,k}^{(i)}$  ( $j = -1, 0, 1, \dots, T-1; k =$   
235  $0, 1, 2, \dots, 2^j-1; i = 1, 2, \dots, p$ ) are the wavelet coefficients for  
236 the  $i$ -th autoregressive coefficient function  $a_{lmi}(t)$ . As the basis  
237 functions  $\phi(t)$  and  $\psi_{j,k}(t)$  are known, the task of estimating the  
238 dynamic autoregressive parameters consists of the estimation of  
239 each of the wavelet coefficients  $c_{j,k}^{(i)}$  for all the autoregressive  
240 functions in the matrices  $\mathbf{A}_i(t)$  ( $i = 1, 2, \dots, p$ ), the intercept  
241 functions in  $\mathbf{v}(t)$  and the covariance functions in  $\Sigma(t)$ . 242

A very important point is the choice of the maximum  
243 resolution scale parameter  $J$ . This task is strongly related to  
244 previous information about the smoothness of the curve to be  
245 estimated. If we desire to capture more details or a high level of  
246 adaptability, a large value of  $J$  has to be chosen. However, there  
247 is a trade off to be considered, as large values of  $J$  imply large  
248 variances. Hence, we concluded that the maximum scale  
249 parameter has to be chosen according to the expected degree of  
250 smoothness of the connectivity changes. 251

Maximum likelihood estimation is not efficient in this case, due  
252 to the large number of parameters to be estimated. [Dahlhaus et al.](#)  
253 (1999) suggested an estimation approach in the univariate case, and  
254 we have generalized it to multivariate time series. We propose the  
255 use of an interactive generalized least square estimation procedure,  
256 which is composed by a loop of two stages. In the first stage, the  
257 parameters of  $\mathbf{A}_i(t)$  and  $\mathbf{v}(t)$  are estimated using a generalized least  
258 square estimation. Then, in the second stage, the covariance  
259 functions in  $\Sigma(t)$  are estimated using the residuals of the first  
260 stage. These two steps are repeated until the convergence of the  
261 parameters, or until a certain number of maximum interactions is  
262 achieved, as an extension of the Cochrane and Orcutt procedure.  
263 Details of the estimation procedure and asymptotical statistical  
264 results are presented in Appendix A. Statistical tests of the  
265 significance of the coefficients and connectivities were undertaken  
266 using Wald tests, and details are also included in Appendix A. In  
267 this work, we chose the extreme phase daubechies 8 wavelet basis  
268 proposed by [Daubechies \(1988\)](#), with periodic boundary con-  
269 ditions, but the results are applicable to any wavelet basis. Optimal  
270 use of wavelets optimal requires a power of 2 time series length. 271

## 272 Simulations

In order to evaluate the DVAR approach to fMRI connectivity  
273 analysis, we simulated 1000 five-dimensional dynamic autore- 274

275 gressive models of order 1. We consider an AB periodic structure  
 276 with six cycles of length 16, assuming that each cycle has the  
 277 same time-varying connectivity structure. Hence, supposing the  
 278 five series are BOLD signals of five different brain areas, we  
 279 evaluated the performance and usefulness of the novel method.  
 280 The model and theoretical functions of these simulations are  
 281 described in Appendix A. The DVAR model estimation procedure  
 282 was applied to the signals in each simulation and the results are  
 283 shown in Fig. 1.

284 The simulations show that the average of each of the  
 285 estimated curves is close to the theoretical ones. Further, the  
 286 estimates do not have a high variability, indicating that the DVAR  
 287 approach has good performance. Consider the connectivity  
 288 function map shown in Fig. 1 as an illustrative example of a  
 289 model to be interpreted. The panel (3->4) indicates the flow of  
 290 information from the third series to the fourth, and the flow is  
 291 higher in the middle of the cycle. The absolute values of the  
 292 connectivity function measure the degree of the flow of  
 293 information. If the connectivity function is negative, it can be  
 294 interpreted as a negative impact, i.e., an increase in the sender's  
 295 signal is followed by a decrease in the receiver's signal.

296 A very important point to be highlighted in these  
 297 simulations is the nonprespecification of connectivity structure.  
 298 All possible connections are considered without any inclusion  
 299 of exogenous variables or subjective assumptions. Thus, if two  
 300 areas are disconnected during all the cycle, the connectivity  
 301 function is zero for each time point as shown in panel (2->5).  
 302 Statistical tests about the parameters of the model can also be

303 tested using a Wald contrast test, which is described in  
 304 Appendix A. Hence, connectivity tests in any time interval  
 305 can be performed. We say that an area A is sending  
 306 information to another area B, if and only if the connectivity  
 307 function from A to B is nonzero. Thus, the Wald test can be  
 308 very useful to inferring the connectivity structure at any time  
 309 point, as the estimated connectivity functions are linear  
 310 combinations of the parameters (contrasts).

### Application to fMRI real data

311  
 312 The DVAR approach was applied to two subjects who performed  
 313 motor tasks in a simple AB block design. The images were acquired  
 314 in a GE 1.5 T Signa MR system equipped with a 23 mT/m gradient  
 315 (TE 40 ms, TR 3000 ms, FA 75°, FOV 240 mm, 64 × 64 matrix;  
 316 8 slices, thickness 7.0 mm, gap 0.7 mm) oriented in the AC–PC  
 317 plane in a single run. Sixty volumes were acquired during three  
 318 cycles of rest-task performance (each one with 60 s and 20 images)  
 319 and the total imaging time for each run was 3:12 min (which  
 320 included 4 TR to achieve steady-state transverse magnetization).  
 321 Both subjects were normal, right-handed females. During the MR  
 322 imaging, the subjects lay in the dark with a noise-reducing  
 323 headphones that were customized for functional MR imaging  
 324 experiments and provide isolation from scanner noise. The AB  
 325 block design experiment paradigm consisted of alternating (condition  
 326 A) rest and (condition B) right hand self-paced finger tapping  
 327 movements.

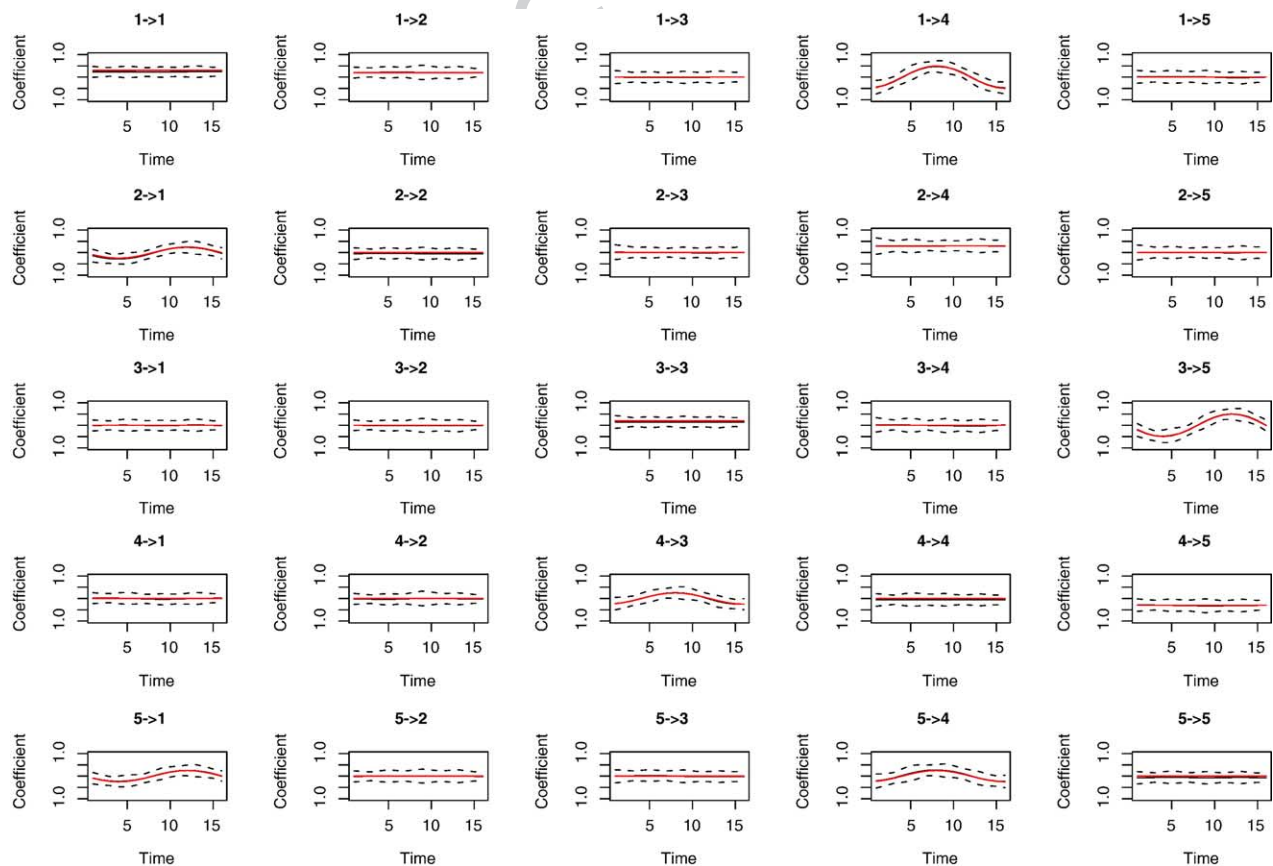


Fig. 1. Simulation results of five-dimensional time series. The solid red line is the theoretical connectivity function  $A_1(t)$  and the solid black line is the average of the estimated curves. The ticked lines are the band of one standard error.

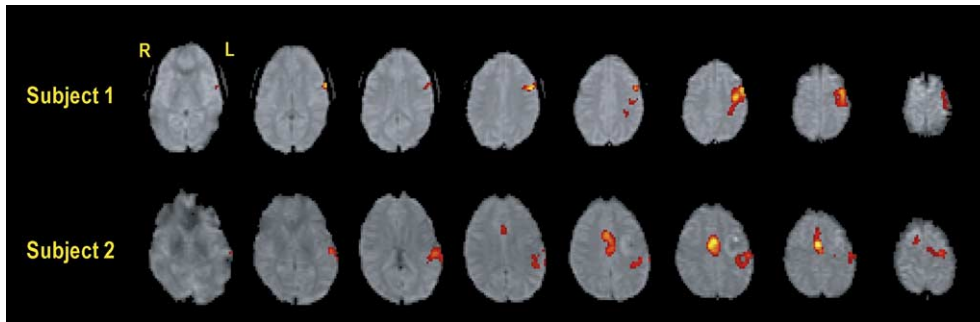


Fig. 2. Activated areas detected during the finger tapping of two subjects in a motor experiment (radiological notation).

328 The volumes were motion corrected and spatially smoothed  
 329 (Brammer et al., 1997). The responses at each voxel were  
 330 modeled by Poisson functions and activation maps were obtained  
 331 using a nonparametric approach (Brammer et al., 1997; Brammer,  
 332 1998; Bullmore et al., 1999, 2001, 2003; Breakspear et al., 2004).  
 333 The areas detected as active (cluster  $P$  value = 0.01) are shown in  
 334 Fig. 2.

335 The first illustration of the use of DVAR to real fMRI data  
 336 involved a multiple bivariate approach. In this analysis, we selected  
 337 one ROI of  $5 \times 5$  voxels centered in the local maximum of the  
 338 primary motor area (M1) in one slice. The three AB cycles  
 339 originally composed by 20 volumes were reduced to 16 volumes by  
 340 cubic splines interpolation, allowing the use of Daubechies periodic  
 341 double extreme phase wavelets. The wavelet DVAR approach of  
 342 order 1 was applied to bivariate models using this ROI average  
 343 signal and each remaining intracerebral voxel. This is a time-  
 344 varying extension of the approach used by Goebel et al. (2003). The  
 345 connectivity maps (Figs. 3 and 4) were smoothed using a Gaussian  
 346 kernel filter (FWHM 5 mm). The maps show the temporal  
 347 information flow intensity changes (from each voxel to the ROI)  
 348 during the AB cycle, measured by the connectivity functions (with  
 349 threshold in absolute values less than 0.9). The maps can also be  
 350 thresholded by computing the value of the estimated connectivity

for significance at a particular chosen  $P$  value, considering the Wald  
 Test (in Appendix A).

The images show a pattern of bivariate relationships with  
 signal variation in prefrontal regions initially explaining the M1  
 time-series variability. This relationship (in the rest phase)  
 evolves to include parietal areas and premotor regions. This  
 slice also shows that signal changes in M1 are also highly  
 predicted by its own previous behavior during both rest and  
 active epochs.

In the second subject, we have also found that areas with  
 signal variations explaining the signal change in M1 occur in the  
 prefrontal cortex during the rest epoch, and proceed to a more  
 parietal and premotor distribution during the active phase.  
 Likewise, the M1 signal change is also predicted by its own  
 history of signal changes, and in this case markedly during the  
 moments where the subject was finger tapping with the contra  
 lateral hand.

The DVAR model can also be applied to preselected ROIs, in  
 a  $k$ -dimensional modeling. We preselected five ROIs from the  
 connectivity maps of subject two, including the local maxima of  
 the left primary motor cortex in the precentral gyrus (LM1), left  
 Anterior Cingulate gyrus (ACg), a medial superior medial frontal  
 gyrus, centered on the Supplementary motor area (SMA), right

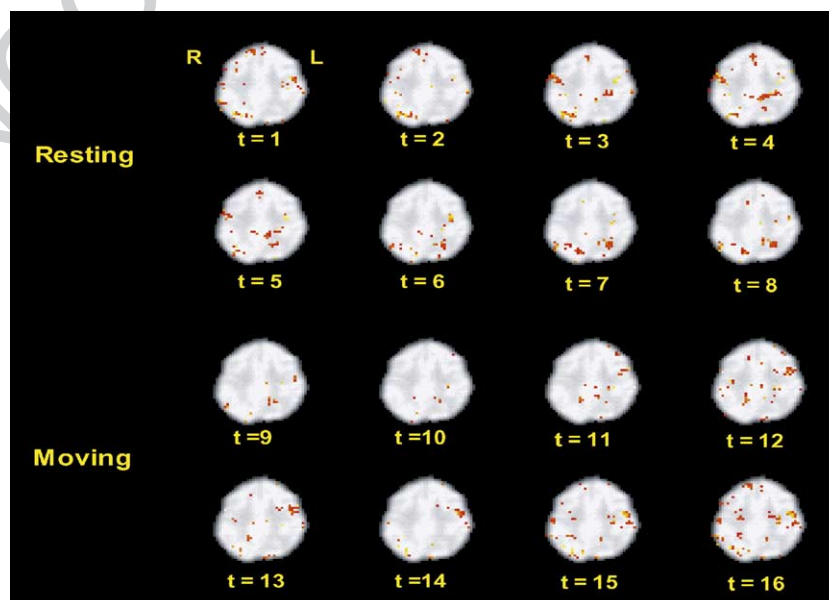


Fig. 3. Subject one connectivity map. The map shows the voxel to ROI information flow intensity, estimated by connectivity functions of the DVAR model.

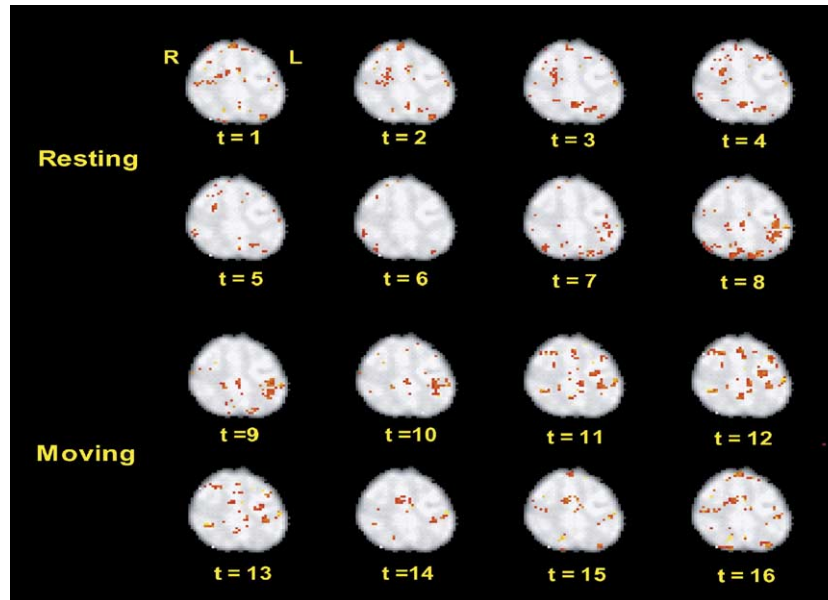


Fig. 4. Subject two connectivity map. The map shows the voxel to ROI information flow intensity, estimated by the connectivity functions.

374 anterior back of the precentral gyrus, the right premotor cortex  
 375 (RpM1) and superior dorsal aspect of the medial parietal lobe, the  
 376 anterior precuneus (ApC). These areas are implied in movement  
 377 control (Kermadi et al., 2000; Wenderoth et al., 2005a,b) and are  
 378 shown to participate in motor learning skills (Jancke et al., 2000;  
 379 Kurata et al., 2000). The DVAR model was modeled to the data  
 380 and a Wald test for significant connectivities (see Appendix A)  
 381 was carried out. The ROI connectivity diagram showing the  
 382 significant links ( $P$  value  $< 0.05$ ) is depicted in Fig. 5.

383 The analysis of the temporal evolution of the connectivity  
 384 between the areas shows an influence of the SMA and ApC in  
 385 the LM1 during the rest period, which is reduced during the  
 386 movement epoch, with a subtle inversion of this influence at the  
 387 first two images of this period. Conversely, the flow of  
 388 information from the LM1 to the RpM1 displays a reversed  
 389 pattern, with most of the BOLD effect predicted (and in opposite  
 390 signal) in the RpM1 during the rest period changing to a positive  
 391 influence during the movement period. The relation between ACg  
 392 and SMA is somewhat more complex, with an enhanced positive  
 393 connectivity in the transitions between rest and movement, and a  
 394 negative connectivity in the rest period, which is even more  
 395 evident in the movement period.

## 396 Discussion

397 The main advantage of the wavelet-based dynamic autoregres-  
 398 sive models (DVAR), compared with other connectivity models is  
 399 that it avoids stationarity and linearity assumptions. It is well  
 400 known that different tasks involve different circuitries, and is  
 401 widely believed that the brain exhibits dynamic alterations in  
 402 interregional connectivity. Hence, the adoption of probably  
 403 unwarranted stationarity assumptions may lead to spurious results.  
 404 Furthermore, the DVAR approach does not require model  
 405 prespecification, unlike structural equation modeling (Buchel and  
 406 Friston, 1997), and this may be desirable as in the illustrations  
 407 above. ROI preselections or prespecification represent particular  
 408 cases of the DVAR model.

Classical dynamic models are based on local fitting using a  
 moving window. However, the detection of dynamic changes by  
 this approach may have poorer time-resolution and be less  
 flexible than that achieved by wavelet-based methods (Dahlhaus  
 et al., 1999). Further, replications of conditions as an AB  
 experiments can be easily modeled by periodic wavelets.

The engagement of prefrontal regions observed in our data as  
 the source of information to the primary motor region is  
 expected during the initial moments of the active epoch, and is  
 consistent with previous studies of motor preparation (Lee et al.,  
 1999; Ohara et al., 2001; Cunnington et al., 2002). The  
 detection of premotor and supplementary areas as ‘predictors’  
 of the BOLD signal change of the primary motor region is also  
 expected, since the involvement of those regions has already  
 been demonstrated in previous studies relating to motor  
 preparation (Cui et al., 2000; D’Esposito et al., 2000; Toni et  
 al., 2001). On the other hand, these regions are constantly  
 sending information to the primary motor cortex across the  
 experiment, which may thus represent a monitoring process, and  
 perhaps could be modulated by habituation, or training,  
 processes. In fact, the left premotor region is evident in the  
 connectivity map only in the active epochs, and is not involved  
 in sending information to the primary motor region in the rest  
 epoch in subject 2.

In addition, towards the end of the “rest” epoch, we detected  
 an increased participation of the parietal regions, possibly related  
 to monitoring of movements (Coull et al., 2000; Hall et al., 2000;  
 Lutz et al., 2000). The prefrontal regions are possibly modulating  
 the information flow to the primary motor region the rest period,  
 especially at the beginning of the epoch. This could be due to an  
 inhibitory process and attentional load, as this area has been  
 described as a putative center for top-down control of the  
 information in the network.

When analyzing the connectivity map from the five predefined  
 regions, the pattern of connectivity is even more interesting, since  
 we have more precise information regarding the signal of the  
 connectivity. It is expected that the BOLD effect in areas  
 hierarchically organized in movement control can be used to infer

409  
 410  
 411  
 412  
 413  
 414  
 415  
 416  
 417  
 418  
 419  
 420  
 421  
 422  
 423  
 424  
 425  
 426  
 427  
 428  
 429  
 430  
 431  
 432  
 433  
 434  
 435  
 436  
 437  
 438  
 439  
 440  
 441  
 442  
 443  
 444  
 445  
 446

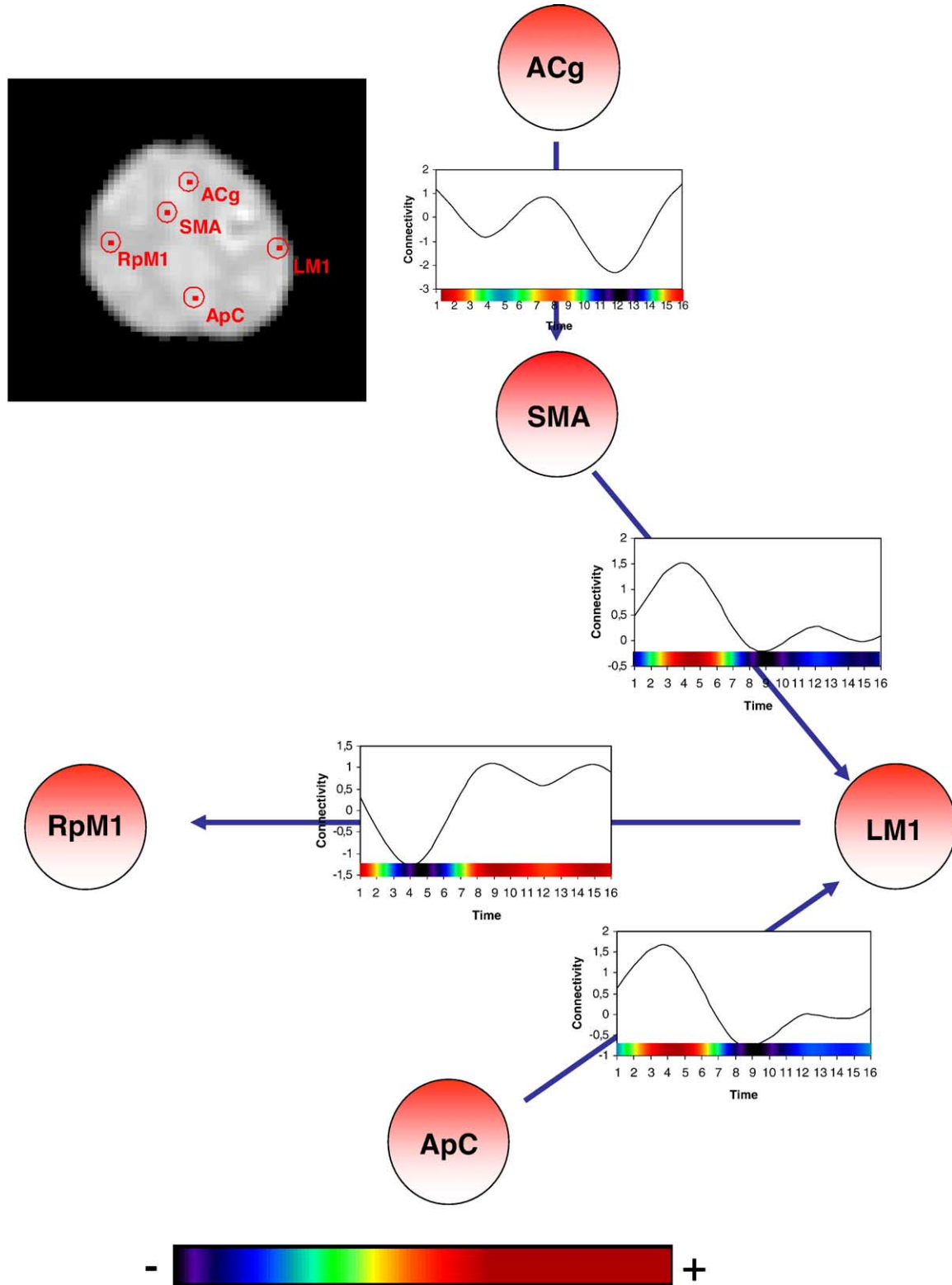


Fig. 5. Significant ROI connectivities. The connectivity functions are shown in each arrow.

447 modulation, or influence, in the BOLD effect in the primary motor  
 448 area. The pattern of temporal evolution found in the connectivity  
 449 map is clearly very elusive in at least one sense: the information flow  
 450 is in agreement to what one can predict from previous studies in  
 451 humans and animal models (Stephan et al., 1999; Kermadi et al.,

2000), although at this point not conclusive. The ACg is believed to  
 452 mediate the processes involved in integration and bimanual control,  
 453 and as well as SMA is involved in both complexity and frequency of  
 454 hand movement (Debaere et al., 2004; Wenderoth et al., 2004,  
 455 2005a,b). The dorsal anterior precuneus region is believed to be  
 456

involved in the attentional aspect of the motor task (Wenderoth et al., 2005a,b). In our analysis, the temporal evolution of the connectivity between this area and the primary motor region suggests that most of its influence is observed in the rest period, perhaps reflecting expectation. One may expect this pattern to change during bimanual tasks (Wenderoth et al., 2005a,b), or even, the fact we are detecting this area as modulating activity in the primary motor area in the rest is congruent and complementary to the concept of its participation in a “default mode network” (Raichle et al., 2001).

Another interesting pattern of connectivity emerging from this preliminary analysis is the supra-periodicity variation of the flow of information between the ACg and SMA. The participation of these areas during the planning of the movement, but not execution of bimanual movements was described by Viallet et al. (1992). Furthermore, SMA region is not unique, and pre-SMA neurons are more active during movement preparation than execution (Matelli et al., 1991; Luppino et al., 1993; Rizzolatti et al., 1996). In our analysis, the flow of information between ACg and SMA is ‘switched on’ during the transitions between conditions, and decays during the middle of the epochs congruent with the idea of participation of these areas in selection of action sets (Rushworth et al., 2004). This type of information could be used to check the assumption that ACg has a modulatory influence in SMA activity in bimanual tasks, as was predicted by the literature (Boecker et al., 1998; Wenderoth et al., 2005a,b).

Clearly, these are preliminary data, but nonetheless they are in reasonable agreement with current opinion in motor planning and execution. We have also used only the original epi images as the source of time-series, instead of using time-series from images previously transformed to a common space. The reason for our choice was to avoid the interference from automatic spatial transformation algorithms, and was based on a high variability of the medial frontal functional regions among subjects (Stephan et al., 1999). Even so, caution should be taken when interpreting the connectivity maps regarding anatomical location of the areas in the model. Although the distinction between SMA and ACg is not defined, even cytoarchitectonic, we used the definition from Stephan et al. (1999) as these authors have described the structures in individual subjects based on anatomical landmarks. Nevertheless, our method does not depend on the adopted procedure for neuroanatomical region selection, and could be used with template brains and Talairach coordinates if the user wishes to (Talairach and Tournoux, 1988).

Although these are very crude observations, it is evident that the method can produce valuable information about brain function as probed by BOLD images. We believe that this analysis may provide useful insights into the investigation of neural networks using fMRI, free from some of the limitations implicit in much existing methodology.

## 505 Conclusion

Understanding neural connectivity is widely recognized as being essential for the understanding of brain function. Nevertheless, the complexity and time-varying properties of cerebral signals sampled by techniques such as fMRI are obstacles for the application of classical stationary models, because different tasks or states demand different brain circuitries and directions of information flow across time. Instead of providing only one connectivity structure for the entire experiment, our technique provides different structures for each time point. We propose a wavelet-based time-varying

connectivity analysis trying to overcome the constraints of stationary models, and illustrated its usefulness with plausible results using real fMRI data sets.

## Uncited reference

Biswal et al., 1995

## Acknowledgments

We like to thank the reviewers for the insightful and useful suggestions. Mr. Sato is supported by CAPES and CNPq/Brazil.

## Appendix A. Estimation algorithm and statistical properties

In this section, the estimation procedure and some useful statistical results are presented. Let  $y_t$ , a  $k$ -dimensional multivariate time series with length  $T$ , modeled by a time-varying VAR process of order  $p$ . Consider the following matrices

$$\mathbf{Y}_{t-l} = \begin{bmatrix} y_{1,(p-l+1)} & y_{2,(p-l+1)} & \cdots & y_{k,(p-l+1)} \\ y_{1,(p-l+2)} & y_{2,(p-l+2)} & \cdots & y_{k,(p-l+2)} \\ \vdots & \vdots & \ddots & \vdots \\ y_{1,(T-l)} & y_{2,(T-l)} & \cdots & y_{k,(T-l)} \end{bmatrix},$$

$$\mathbf{U} = \begin{bmatrix} \mathbf{u}_{1,(p+1)} & \mathbf{u}_{2,(p+1)} & \cdots & \mathbf{u}_{k,(p+1)} \\ \mathbf{u}_{1,(p+2)} & \mathbf{u}_{2,(p+2)} & \cdots & \mathbf{u}_{k,(p+2)} \\ \vdots & \vdots & \ddots & \vdots \\ \mathbf{u}_{1,T} & \mathbf{u}_{2,T} & \cdots & \mathbf{u}_{k,T} \end{bmatrix}$$

and

$$\mathbf{\Pi} = \begin{bmatrix} \psi_{-1,0}(p+1) & \psi_{0,0}(p+1) & \cdots & \psi_{J,2^J-1}(p+1) \\ \psi_{-1,0}(p+2) & \psi_{0,0}(p+2) & \cdots & \psi_{J,2^J-1}(p+2) \\ \vdots & \vdots & \ddots & \vdots \\ \psi_{-1,0}(T) & \psi_{0,0}(T) & \cdots & \psi_{J,2^J-1}(T) \end{bmatrix}.$$

Let also the row-Kronecker product defined by

$$\begin{bmatrix} a_1 \\ a_2 \\ \vdots \\ a_n \end{bmatrix} \otimes^L \begin{bmatrix} b_1 \\ b_2 \\ \vdots \\ b_n \end{bmatrix} = \begin{bmatrix} a_1 & b_1 \\ b_2 & b_2 \\ \vdots & \vdots \\ a_n & b_n \end{bmatrix},$$

and the following matrices

$$\mathbf{W} = \left[ \mathbf{1}_{T-p} \otimes^L \mathbf{\Pi} \mathbf{Y}_{t-1} \otimes^L \mathbf{\Pi} \cdots \mathbf{Y}_{t-l} \otimes^L \mathbf{\Pi} \right],$$

$$\mathbf{M} = \mathbf{I}_k \otimes \mathbf{W},$$

where  $\mathbf{1}_{T-p}$  is a column vector of  $(T-p)$  ones and  $\mathbf{I}_k$  is identity matrix of order  $k$ .

Considering that the wavelet expansion of an information flow function from the series  $y_{lt}$  to  $y_{mt}$  is given by

$$a_{lmi}(t) = \sum_{j=-\infty}^{\infty} \sum_{k=-\infty}^{\infty} c_{j,k}^{(i)} \psi_{j,k}(t),$$

$$(j = -1, 0, 1, \dots, T-1; k = 0, 1, 2, \dots, 2^j - 1; i = 1, 2, \dots, p),$$

515  
516  
517

518

519

520

521

522

523

524

525

526

527

528

530

533

534

536

537

538

539



540 and hence, assuming that the random errors covariance matrix  $\Sigma(t)$   
542 for all  $t$  is known and considering the vector

$$Z = \text{vec}(\mathbf{Y}_t),$$

543 the DVAR model can be written as

$$Z = \mathbf{M}\mathbf{b} + \varepsilon.$$

546 The parameter  $\beta$  is a vector containing all the wavelet  
548 expansion coefficients  $c_{j,k}^{(i)}$  for all the connectivity functions to be  
549 estimated. The error term  $\varepsilon = \text{vec}(\mathbf{U})$  is a vector containing all the  
550 random errors of all the  $k$  series. The covariance matrix of  $\varepsilon$  is  
551 denoted by  $\Gamma$ , contains all covariance the matrices  $\Sigma(t)$  ( $t = p, p +$   
552  $1, \dots, T$ ) and is time-invariant.

553 Hence, from Graybill (1976), the generalized least square  
554 estimator for the parameters of the model is given by

$$\hat{\beta}(\mathbf{M}' \Gamma^{-1} \mathbf{M})^{-1} \mathbf{M}' \Gamma^{-1} Z.$$

556 In practice, the error covariance matrix is unknown and it has  
558 to be estimated. A consistent estimator for the time-varying  
559 variance for each time series can be obtained considering a  
560 wavelet smoothing of the squared residuals ( $r_{it}^2$ ,  $i = 1, \dots, k$ ).  
561 Furthermore, the time-varying covariances can also be obtained  
562 by a wavelet smoothing of the cross-residuals ( $r_{it}r_{jt}$ ,  $i = 1, \dots, k$ ,  
563  $j = 1, \dots, k$ ,  $i \neq j$ ).

564 Hence, we propose an interactive algorithm given by:

565

- 566 (1) Assume  $\Gamma = \mathbf{I}$ , and perform the generalized least square  
567 estimation;
- 568 (2) Compute the residuals and obtain an estimate of the errors  
569 time-varying covariance matrix;
- 570 (3) Perform the generalized least square estimation considering  
571 the estimated covariance matrix;
- 572 (4) Go to step 2 and repeat until the convergence of the  
573 parameters.

574

575 Considering the estimation procedure described, it can be  
576 shown (see Hajek-Sidak's Central Limit Theorem, Sen and Singer,  
577 1980) that the asymptotic distribution of the interactive generalized  
578 least square estimator is given by

$$\sqrt{kT}\hat{\beta} \sim N(\beta, \Gamma).$$

580 Furthermore, the statistical test to the null hypothesis of

$$\mathbf{C}\beta = m,$$

583 against the hypothesis of inequality can be tested using the Wald  
584 Statistic for contrasts given by

$$W = \frac{(\mathbf{C}\hat{\beta} - m)' [\mathbf{M}' \Gamma^{-1} \mathbf{M}]^{-1} (\mathbf{C}\hat{\beta} - m)}{\text{rank}(\mathbf{C})},$$

586 where  $\mathbf{C}$  is the contrast matrix.

587 Hence, we can test many hypothesis of connectivity  
588 significance or time-varying connectivity performing a Wald  
589 test, considering an adequate contrast matrix  $\mathbf{C}$ . More details  
590 about the Wald test for contrasts can be found in Graybill  
591 (1976). Any statistical test for the connectivity functions can be  
592 performed using the Wald test, as the functions are estimated  
593 by linear combinations of the coefficients. For example, the  
594 statistical test for a link between two regions can be performed

considering the hypothesis that all wavelets expansion coef- 595  
ficients for this connectivity function are zero. 596

In addition, we can also obtain confidence intervals for the 597  
connectivity functions. Let  $\hat{\xi}$  a vector containing all estimated 598  
coefficients for a wavelet expansion of a function  $f(t)$ ,  $\delta(t)$  a vector 599  
of the respective wavelets functions in time  $t$  and  $\Lambda$  the covariance 600  
matrix of  $\hat{\xi}$ . A natural estimator of  $f(t)$  is given by 601

$$\hat{f}(t) = \hat{\xi}' \delta(t)$$

It can be shown, using Hajek-Sidak's Central Limit Theorem 602  
(Sen and Singer, 1980) that asymptotically 605

$$\hat{f}(t) \sim N(f, \delta \Lambda \delta'),$$

and hence, confidence intervals for each connectivity function can 608  
be obtained using this result. 609

### Simulations 610

In the Simulations section, we consider a DVAR model of order 611  
one, considering the following connectivity matrix 612

$$\mathbf{A}(t) = \begin{bmatrix} 0 & 0.2 & 0 & \cos(\frac{2\pi t}{16} + \pi)/2 & 0 \\ \sin(\frac{2\pi t}{16} + \pi)/4 & 0 & 0 & 0.3 & 0 \\ 0 & 0 & 0.2 & 0 & \sin(\frac{2\pi t}{16} + \pi)/2 \\ 0 & 0 & \cos(\frac{2\pi t}{16} + \pi)/4 & 0 & 0.3 \\ \sin(\frac{2\pi t}{16} + \pi)/4 & 0 & 0 & \cos(\frac{2\pi t}{16} + \pi)/4 & 0 \end{bmatrix},$$

intercept vector given by 613

$$\mathbf{v}(t) = \begin{bmatrix} \sin(\frac{2\pi t}{16} + \pi)/2 \\ 0 \\ \cos(\frac{2\pi t}{16} + \pi)/4 \\ 0 \\ 0 \end{bmatrix},$$

and error covariance matrix 616

$$\Sigma(t) = \begin{bmatrix} 0.49 & 0.147(1 + \cos(\frac{2\pi t}{16})/6) & 0 & 0 & 0 \\ 0.147(1 + \cos(\frac{2\pi t}{16})/6) & 0.53(1 + \cos(\frac{2\pi t}{16})/6) & 0 & 0 & 0 \\ 0 & 0 & 0.49 & 0 & 0 \\ 0 & 0 & 0 & 0.49 & 0.0147 \\ 0 & 0 & 0 & 0.147 & 0.6341 \end{bmatrix}. 618$$

### References 619

- Baccala, L.A., Sameshima, K., 2001. Partial directed coherence: a 621  
new concept in neural structure determination. *Biol. Cybern.* 84 (6), 622  
463–474. 623
- Biswal, B., Yetkin, F.Z., et al., 1995. Functional connectivity in the motor 624  
cortex of resting human brain using echo-planar MRI. *Magn. Reson.* 625  
*Med.* 34 (4), 537–541. 626
- Boecker, H., Dagher, A., et al., 1998. Role of the human rostral 627  
supplementary motor area and the basal ganglia in motor sequence 628  
control: investigations with H2 15O PET. *J. Neurophysiol.* 79 (2), 629  
1070–1080. 630
- Brammer, M.J., 1998. Multidimensional wavelet analysis of 631  
functional magnetic resonance images. *Hum. Brain Mapp.* 6 (5–6), 632  
378–382. 633
- Brammer, M.J., Bullmore, E.T., et al., 1997. Generic brain activation 634  
mapping in functional magnetic resonance imaging: a nonparametric 635  
approach. *Magn. Reson. Imaging* 15 (7), 763–770. 636
- Breakspear, M., Brammer, M.J., et al., 2004. Spatiotemporal wavelet 637  
resampling for functional neuroimaging data. *Hum. Brain Mapp.* 23 (1), 638  
1–25. 639

- 640 Buchel, C., Friston, K.J., 1997. Modulation of connectivity in visual  
641 pathways by attention: cortical interactions evaluated with structural  
642 equation modelling and fMRI. *Cereb. Cortex* 7 (8), 768–778.
- 643 Bullmore, E.T., Suckling, J., et al., 1999. Global, voxel, and cluster tests, by  
644 theory and permutation, for a difference between two groups of  
645 structural MR images of the brain. *IEEE Trans. Med. Imag* 18 (1),  
646 32–42.
- 647 Bullmore, E., Long, C., et al., 2001. Colored noise and computational  
648 inference in neurophysiological (fMRI) time series analysis: resam-  
649 pling methods in time and wavelet domains. *Hum. Brain Mapp.* 12 (2),  
650 61–78.
- 651 Bullmore, E., Fadili, J., et al., 2003. Wavelets and statistical analysis of  
652 functional magnetic resonance images of the human brain. *Stat.*  
653 *Methods Med. Res.* 12 (5), 375–399.
- 654 Bullmore, E., Fadili, J., et al., 2004. Wavelets and functional magnetic  
655 resonance imaging of the human brain. *NeuroImage* 23 (Suppl. 1),  
656 S234–S249.
- 657 Chang, C., Moretting, P.A., 2005. Time domain estimation of time-varying  
658 linear systems. *J. Nonparametr. Stat.* 17, 365–383.
- 659 Coull, J.T., Frith, C.D., et al., 2000. Orienting attention in time: behavioural  
660 and neuroanatomical distinction between exogenous and endogenous  
661 shifts. *Neuropsychologia* 38 (6), 808–819.
- 662 Cui, S.Z., Li, E.Z., et al., 2000. Both sides of human cerebellum involved in  
663 preparation and execution of sequential movements. *NeuroReport* 11  
664 (17), 3849–3853.
- 665 Cunnington, R., Windischberger, C., et al., 2002. The preparation and  
666 execution of self-initiated and externally-triggered movement: a study  
667 of event-related fMRI. *NeuroImage* 15 (2), 373–385.
- 668 Dahlhaus, R., Neumann, M.H., et al., 1999. Nonlinear wavelet estimation of  
669 time-varying autoregressive processes. *Bernoulli* 5 (5), 873–906.
- 670 Daubechies, I., 1988. Orthonormal bases of compactly supported wavelets.  
671 *Commun. Pure Appl. Math.* 41, 909–996.
- 672 Debaere, F., Wenderoth, N., et al., 2004. Changes in brain activation during  
673 the acquisition of a new bimanual coordination task. *Neuropsychologia*  
674 42 (7), 855–867.
- 675 D’Esposito, M., Ballard, D., et al., 2000. The role of prefrontal cortex in  
676 sensory memory and motor preparation: an event-related fMRI study.  
677 *NeuroImage* 11 (5 Pt. 1), 400–408.
- 678 Eichler, M., 2005. A graphical approach for evaluating effective connec-  
679 tivity in neural systems. *Philos. Trans. R. Soc. Lond., Ser. B Biol. Sci.*  
680 29;360 (1457), 953–967.
- 681 Friston, K.J., 1995. Functional and effective connectivity in neuroimaging:  
682 a synthesis. *Hum. Brain Mapp.* 2 (2), 56–78.
- 683 Friston, K., 2002. Beyond phrenology: what can neuroimaging tell us about  
684 distributed circuitry? *Annu. Rev. Neurosci.* 25, 221–250.
- 685 Friston, K.J., Harrison, L., et al., 2003. Dynamic causal modelling.  
686 *NeuroImage* 19 (4), 1273–1302.
- 687 Geweke, J., 1982. Measuring linear dependence and feedback between  
688 multiple time series. *JASA* 77 (378), 304–313.
- 689 Goebel, R., Roebroeck, A., et al., 2003. Investigating directed cortical  
690 interactions in time-resolved fMRI data using vector autoregressive  
691 modeling and Granger causality mapping. *Magn. Reson. Imaging* 21  
692 (10), 1251–1261.
- 693 Granger, C.W.J., 1969. Investigating causal relations by econometric  
694 models and cross-spectral methods. *Econometrica* 37, 424–438.
- 695 Graybill, F.A., 1976. *Theory and Application of the Linear Model*. A:  
696 Duxbury, North Scituate.
- 697 Hall, D.A., Haggard, M.P., et al., 2000. Modulation and task effects in  
698 auditory processing measured using fMRI. *Hum. Brain Mapp.* 10 (3),  
699 107–119.
- 700 Jancke, L., Himmelbach, M., et al., 2000. The effect of switching between  
701 sequential and repetitive movements on cortical activation. *NeuroImage*  
702 12 (5), 528–537.
- 703 Kermedi, I., Liu, Y., et al., 2000. Do bimanual motor actions involve the  
704 dorsal premotor (PMd), cingulate (CMA) and posterior parietal (PPC)  
705 cortices? Comparison with primary and supplementary motor cortical  
706 areas. *Somatosens Mot. Res.* 17 (3), 255–271.
- Kurata, K., Tsuji, T., et al., 2000. Activation of the dorsal premotor cortex  
707 and pre-supplementary motor area of humans during an auditory  
708 conditional motor task. *J. Neurophysiol.* 84 (3), 1667–1672.
- 709 Lee, K.M., Chang, K.H., et al., 1999. Subregions within the supplementary  
710 motor area activated at different stages of movement preparation and  
711 execution. *NeuroImage* 9 (1), 117–123.
- 712 Luppino, G., Matelli, M., et al., 1993. Corticocortical connections of area  
713 F3 (SMA-proper) and area F6 (pre-SMA) in the macaque monkey. *J.*  
714 *Comp. Neurol.* 338 (1), 114–140.
- 715 Lütkepohl, H., 1993. *Introduction to Multiple Time Series Analysis*. (2nd  
716 edition) Springer, Berlin.
- 717 Lutz, K., Specht, K., et al., 2000. Tapping movements according to regular  
718 and irregular visual timing signals investigated with fMRI. *NeuroReport*  
719 11 (6), 1301–1306.
- 720 Matelli, M., Luppino, G., et al., 1991. Architecture of superior and mesial  
721 area 6 and the adjacent cingulate cortex in the macaque monkey. *J.*  
722 *Comp. Neurol.* 311 (4), 445–462.
- 723 Ogawa, S., Lee, T.-M., et al., 1990. Oxigenation-sensitive contrast in  
724 magnetic resonance image of rodent brain at high magnetic fields. *J.*  
725 *Magn. Reson. Med.* 14, 68–78.
- 726 Ohara, S., Mima, T., et al., 2001. Increased synchronization of cortical  
727 oscillatory activities between human supplementary motor and primary  
728 sensorimotor areas during voluntary movements. *J. Neurosci.* 21 (23),  
729 9377–9386.
- 730 Raichle, M.E., MacLeod, A.M., et al., 2001. A default mode of brain  
731 function. *Proc. Natl. Acad. Sci. U. S. A.* 98 (2), 676–682.
- 732 Rizzolatti, G., Luppino, G., et al., 1996. The classic supplementary  
733 motor area is formed by two independent areas. *Adv. Neurol.* 70,  
734 45–56.
- 735 Roebroeck, A., Formisano, E., et al., 2005. Mapping directed influence  
736 over the brain using Granger causality and fMRI. *NeuroImage* 25 (1),  
737 230–242.
- 738 Rushworth, M.F., Walton, M.E., et al., 2004. Action sets and  
739 decisions in the medial frontal cortex. *Trends Cogn. Sci.* 8 (9),  
740 410–417.
- 741 Sameshima, K., Baccala, L.A., 1999. Using partial directed coherence to  
742 describe neuronal ensemble interactions. *J. Neurosci. Methods* 94 (1),  
743 93–103.
- 744 Sen, P.K., Singer, J.M., 1980. *Large Sample Methods in Statistics—An*  
745 *Introduction with Applications*. Chapman and Hall, London. (3.  
746 Serfling, R.J).
- 747 Stephan, K.M., Binkofski, F., et al., 1999. The role of ventral medial wall  
748 motor areas in bimanual co-ordination. A combined lesion and  
749 activation study. *Brain* 122 (Pt. 2), 351–368.
- 750 Talairach, J., Tournoux, P., 1988. *Co-Planar Stereotaxic Atlas of the Human*  
751 *Brain: 3-Dimensional Proportional System: An Approach to Cerebral*  
752 *Imaging*. Thieme Medical Pub.
- 753 Toni, I., Thoenissen, D., et al., 2001. Movement preparation and motor  
754 intention. *NeuroImage* 14 (1 Pt. 2), S110–S117.
- 755 Viallet, F., Massion, J., et al., 1992. Coordination between posture and  
756 movement in a bimanual load lifting task: putative role of a medial  
757 frontal region including the supplementary motor area. *Exp. Brain Res.*  
758 88 (3), 674–684.
- 759 Wenderoth, N., Debaere, F., et al., 2004. Parieto-premotor areas mediate  
760 directional interference during bimanual movements. *Cereb. Cortex* 14  
761 (10), 1153–1163.
- 762 Wenderoth, N., Debaere, F., et al., 2005. The role of anterior cingulate  
763 cortex and precuneus in the coordination of motor behaviour. *Eur. J.*  
764 *Neurosci.* 22 (1), 235–246.
- 765 Wenderoth, N., Debaere, F., et al., 2005. Spatial interference  
766 during bimanual coordination: differential brain networks associ-  
767 ated with control of movement amplitude and direction. *Hum.*  
768 *Brain Mapp.*
- 769
- 770